Pergamon

Int. J. Heat Mass Transfer. Vol. 38, No. 7, pp. 1285–1296, 1995

0017–9310/95 $9.50+0.00

0017–9310(94)00237–1

Extension of the continuum model for transport phenomena occurring during metal alloy solidification—II. Microscopic considerations

J. NI and F. P. INCROPERA†

Heat Transfer Laboratory, School of Mechanical Engineering, Purdue University, West Lafayette, IN 47907, U.S.A.

(*Received* 29 *December* 1993 *and in final form* 19 *July* 1994)

Abstract—In a companion paper, a continuum model for simulating transport phenomena occurring during solidification of a binary metal alloy is extended to allow for treatment of effects such as solutal undercooling and solid transport in the form of floating and settling crystals. However, inclusion of such features requires auxiliary models which, in large part, depend on microscopic considerations. Such models are developed in this study and specifically deal with relations for solid and liquid velocities under conditions involving solid motion, as well as determination of solutal undercooling as a function of the solidification rate and stereological characteristics of the solid/liquid interface. The models also permit determination of final grain density and size.

1. INTRODUCTION

In a companion paper [1], models for simulating transport phenomena occurring during solidification of a binary alloy are reviewed, with emphasis placed on existing continuum and two-phase approaches. Linkages between the two approaches are discussed, and volume-averaging procedures inherent in the two-phase model are used to develop an extension to the continuum model which retains its computational convenience, while allowing it to treat effects such as solid movement and solutal undercooling. In this study, auxiliary models are developed to facilitate inclusion of such effects.

During solidification, crystal fragments may fracture from dendrite arms and be advected into a relatively high temperature region in which they may melt to form small nuclei. In turn, the movement of equiaxed crystals may be characterized by settling or floating within the melt, with some crystals experiencing packing and/or attachment to the front formed by stationary columnar dendrites. Moreover, packing or attachment to the front of columnar dendritic tips may initiate a transition from columnar to equiaxed structures (CET). Such features (illustrated in Fig. 1 of ref. [1]) should be considered in modeling solid movement.

One approach to accounting for solid movement in a dispersed flow is to impose a relationship between the solid and liquid velocities, as, for example, through the 'consolidation factor' F introduced by Flood *et al.* [2]. A linear relation is proposed:

$$\mathbf{V}_s = F\mathbf{V}_l \tag{1}$$

where

$$F = \left(1 - \frac{g_s}{g_s^*}\right) \quad \text{for } g_s < g_s^*$$

and

$$F = 0 \quad \text{for } g_s \geqslant g_s^* \tag{2}$$

and g_s^* is a prescribed value of the solid volume fraction corresponding to $\mathbf{V}_s = 0$. In a more recent study, Flood *et al.* [3] implemented this concept in a numerical simulation to investigate the effect of solid movement on macrosegregation. However, except for extremes at $g_s = 0$ and $g_s = g_s^*$, the concept of a linear consolidation factor lacks a physical basis. For stationary columnar structures, g_s^* can be taken as zero. For equiaxed solidification, g_s^* may be interpreted as a maximum solid packing fraction, above which grains merge and solid motion is terminated. However, before the solid crystals reach a packing state for which $\mathbf{V}_s = 0$, they can be floating or settling in the melt, and the concept of a consolidation factor is unable to account for such motion.

In the mixture continuum model [1], an extra relationship is needed to account for the movement of dispersed solid crystals in the melt and should be consistent with the solid and liquid momentum equations. Since solid movement depends on the gravitational field, and possibly other forces characterized by different directional components, the solid transport model should allow for consideration of motion in different directions. In the vertical direction, the buoyancy force may be important and sedimentation and floating should be considered, while in the hori-

† Author to whom correspondence should be addressed.

NOMENCLATURE

- a constant in equations (21) and (22); exponent in equation (27); constant in equation (34)
- A area
- b constant in equations (21) and (22); exponent in equation (34)
- c exponent in equation (34)
- d_s characteristic diameter of solid crystals
- D mass diffusion tensor of a species in the multi-component mixture
- f^α species concentration of a binary mixture (defined in terms of species mass fraction)
- Δf^α difference between interfacial and volumetric species concentrations
- f mass fraction of solid or liquid phase
- F consolidation factor
- $g, \mathbf{g}$ volume fraction of solid or liquid phase; gravitational acceleration
- l diffusion length
- $\mathbf{M}$ interfacial momentum transfer rate per unit volume
- n number of crystals per unit volume or per unit area
- $\dot{n}$ nucleation rate
- p pressure
- Pe macroscopic solutal Peclet number
- $\dot{R}$ local growth rate of interface
- Re multiphase Reynolds number
- R_f final grain radius
- Sc Schmidt number
- S_v interfacial area concentration
- t time
- T equilibrium temperature
- ΔT nucleation undercooling of the liquid melt
- ΔT_σ standard deviation of nucleation undercooling
- ΔT_{nu} mean nucleation undercooling
- u x-velocity component in a Cartesian system
- v y-velocity component in a Cartesian system
- $\mathbf{V}$ velocity
- V_0 control volume
- w_e local growth velocity at the interface of an equivalent envelope of solid structure
- $\mathbf{W}$ mean growth rate of interface
- x integral variable
- y y-coordinate of a Cartesian system.

Greek symbols

- δ local thickness of solutal boundary layer in front of solid/liquid interface
- Γ phase change rate per unit volume
- κ_p segregation coefficient
- λ_1 primary dendrite arm spacing
- μ dynamic viscosity
- ρ average mass density.

Subscripts

- 1 previous time step
- 2 nucleation terminated
- con contacting
- i interface
- l liquid phase
- ld liquidus line
- m mixture
- max maximum
- nu nucleation
- s solid phase
- sp solid packing.

Superscripts

- A per unit area
- c columnar
- d dissipative
- e equiaxed
- j species transfer
- 0 previous time
- α α species component of a binary alloy
- β β species component of a binary alloy
- * effective or macroscopic; prescribed value.

zontal direction solid movement due to phase change and viscous drag may be dominant. In this study, solid transport equations which account for the sedimentation or floating of dispersed crystals in the vertical direction, as well as movement due to phase change and viscous effects, are developed.

Although nonequilibrium effects due to solutal undercooling are important and are considered in microscopic models of solidification, they have been neglected in many of the macroscopic models. Increasingly, however, it is recognized that solutal undercooling effects should be considered. A micro–macroscopic model for equiaxed solidification [4] accounts for solutal undercooling through the kinetic law used to calculate solid volume fraction in the latent heat release source term. However, none of the present micro–macroscopic models include convection effects in the liquid. In the two-phase model developed by Ni and Beckermann [5], the liquid concentration is treated as a dependent variable and the interfacial

liquid concentration is calculated by using the equilibrium interfacial temperature with relations based on the phase diagram. Use of the model by Ni and Beckermann [6] indicates that solutal undercooling has a strong effect on equiaxed solidification, especially at the solidification front.

Solutal undercooling, defined as the difference between the interfacial and volume-averaged liquid species concentrations, $\Delta f_l^\alpha = f_{li}^\alpha - f_l^\alpha$, is strongly influenced by species diffusion in the liquid at the interface. Hence, it may depend on the liquid species diffusivity, the mean crystal and dendrite growth rate, the mean thickness of the solutal boundary layer, the solid volume fraction, and the interfacial area concentration representing the interfacial geometry. However, transport in the liquid and the solutal boundary layer is strongly influenced by convection, which acts to thin the solutal boundary layer at the interface. On the microscopic scale, the effect of solute build-up or local solutal undercooling may be treated through an effective partition (segregation) coefficient κ_p^*, which has been used in metallurgical analyses of microsegregation [7]. Recently Tewari and Shah [8] and Tewari *et al.* [9] utilized the effective partition coefficient model, originally developed by Burton *et al.* [10], to account for solutal undercooling at the dendrite tip region (or growth front) in their study of macrosegregation, and predicted results were in reasonable agreement with experimental data.

The equilibrium partition coefficient relates the interfacial species concentrations of the liquid and solid phases as

$$\kappa_p = \frac{f_{si}^\alpha}{f_{li}^\alpha} \tag{3}$$

and the effective partition coefficient is defined as [7, 11]

$$\kappa_p^* = \frac{f_{si}^\alpha}{f_l^\alpha}. \tag{4}$$

Thus, the liquid solutal undercooling can be expressed as

$$\Delta f_l^\alpha = f_{li}^\alpha - f_l^\alpha = f_{si}^\alpha \left(\frac{1}{\kappa_p} - \frac{1}{\kappa_p^*}\right). \tag{5}$$

Relationships between the effective partition coefficient, liquid species concentration, and the interfacial species concentrations of the solid and liquid phases are illustrated schematically in Fig. 1. From the work of Burton *et al.* [10], Flemings [7] provides the following expression for the effective partition coefficient

$$\kappa_p^* = \frac{\kappa_p}{\kappa_p + (1-\kappa_p)\exp(-\dot{R}\,\delta/D_l)} \tag{6}$$

where $\dot{R}$ is the local crystal growth rate and δ is the thickness of the solutal boundary layer on a microscopic scale. The exponential term accounts for solutal undercooling, where the parameter $\dot{R}\,\delta/D_l$ may be interpreted as a local solutal Peclet number. On a macroscopic scale, $\dot{R}\,\delta/D_l$ may be equated to $\Gamma_s l_l^i/\rho_s D_l S_v$, which may be interpreted as a macroscopic solutal Peclet number *Pe*. The liquid species diffusion length l_l^i characterizes mean species diffusion in the liquid adjoining the solid/liquid interface within a control volume. The physical basis of this macroscopic quantity was provided in the two-phase model of Ni *et al.* [12]. The interfacial area concentration, S_v, is defined as the ratio of the solid/liquid interface area to the control volume, A_i/V_0, and characterizes first-order geometric effects on the interfacial species transfer. In general, S_v is a function of the solid volume fraction and interface geometry.

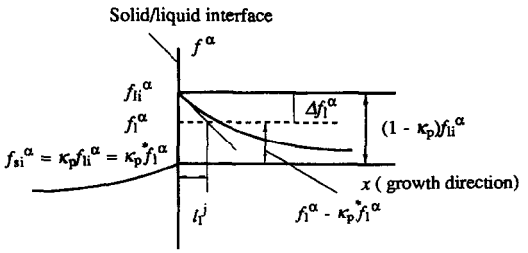

Fig. 1. Schematic illustration of effective partition coefficient κ_p^*, liquid species diffusion length l_l^i, and liquid solutal undercooling Δf_l^α.

In this study equations (5) and (6) are used as a starting point for determining solutal undercooling. The subsequent analysis requires determination of characteristic lengths for the solid structures (equiaxed crystals or columnar dendrites), as well as models for crystal nucleation and fragmentation.

2. MODEL EQUATIONS

2.1. *Solid transport*

A relation for relative motion between the liquid and solid phases may be developed from their respective momentum equations, which appear as equations (6) and (21) in the companion paper [1]. The final form depends on the coordinate direction.

2.1.1. *Solid transport due to floating and sedimentation in vertical direction.* Writing the interfacial momentum balance as $\mathbf{M}_s^d = -\mathbf{M}_l^d - \mathbf{V}_{li}\Gamma_l - \mathbf{V}_{si}\Gamma_s$ and expressing the liquid momentum transfer term, $\mathbf{M}_l^d$, in terms of a drag coefficient, the liquid and solid momentum equations, equations (6) and (21) of ref. [1], can be expressed as follows for the vertical direction:

$$\frac{\partial}{\partial t}(g_l\rho_l v_l) + \nabla\cdot(g_l\rho_l \mathbf{V}_l v_l) = -g_l\frac{\partial p_l}{\partial y} + \frac{3}{4d_s^2}(24)g_s\mu_m(v_s - v_l) - \left(v_s - \frac{(\rho_l-\rho_s)\Gamma_s}{\rho_s\rho_l S_v^2}\frac{\partial g_s}{\partial y}\right)\Gamma_s - g_l\rho_l g + \nabla\cdot\{\mu_l^*[\nabla(g_l v_l) + v_{li}\nabla g_s]\} \tag{7}$$

and

$$\frac{\partial}{\partial t}(g_s\rho_s v_s)+\nabla\cdot(g_s\rho_s \mathbf{V}_s v_s)$$
$$=-g_s\frac{\partial p_s}{\partial y}-\frac{3}{4d_s^2}(24)g_s\mu_m(v_s-v_l)$$
$$+\left(v_s-\frac{(\rho_l-\rho_s)\Gamma_s}{\rho_s\rho_l S_v^2}\frac{\partial g_s}{\partial y}\right)\Gamma_s-g_s\rho_s g+\nabla$$
$$\cdot\{\mu_s^*[\nabla(g_s v_s)-v_{si}\nabla g_s]\}. \quad (8)$$

However, assuming the macroscopic viscous terms to be negligible for the solid and liquid phases of a suspension or a particulate two-phase flow [13], and neglecting inertia effects and interfacial momentum transfer due to phase change relative to interfacial momentum transfer and buoyancy forces, the momentum equations reduce to

$$0=-g_l\frac{\partial p_l}{\partial y}+\frac{3}{4d_s^2}(24)g_s\mu_m(v_s-v_l)-g_l\rho_l g \quad (9)$$

and

$$0=-g_s\frac{\partial p_s}{\partial y}-\frac{3}{4d_s^2}(24)g_s\mu_m(v_s-v_l)-g_s\rho_s g. \quad (10)$$

Equation (10) can be rewritten as

$$\frac{\partial p_s}{\partial y}=-\frac{3}{4d_s^2}(24)\mu_m(v_s-v_l)-\rho_s g. \quad (11)$$

Since the solid particles or crystals are not in contact with each other, pressure equilibrium allows for substitution of equation (11) into equation (9), yielding

$$0=-g_l\left[-\frac{3}{4d_s^2}(24)\mu_m(v_s-v_l)-\rho_s g\right]$$
$$+\frac{3}{4d_s^2}(24)g_s\mu_m(v_s-v_l)-g_l\rho_l g. \quad (12)$$

Hence, with $g_l+g_s=1$, the following relationship between the vertical components of the solid and liquid velocities is obtained:

$$v_s-v_l=\frac{(1-g_s)}{18g_s\mu_m}(\rho_l-\rho_s)d_s^2 g \quad (13)$$

where positive v corresponds to motion in the upward direction. This result is similar to the model proposed by Weinberg [14], which has been verified experimentally. Substituting for the mixture viscosity from equation (17) of ref. [1], it follows that:

$$v_s-v_l=\frac{(1-g_s)\left(1-\dfrac{g_s}{g_{sp}}\right)^{2.5g_{sp}}}{18g_s\mu_l}(\rho_l-\rho_s)d_s^2 g. \quad (14)$$

The foregoing relation accounts for settling by allowing the relative velocity in the vertical direction to be influenced by the buoyancy force and relates settling to the difference between the solid and liquid densities. If $\rho_s>\rho_l$, settling occurs; otherwise the solid crystals or fragments are floating or ascending. Since density differences between the solid and liquid phases vary with temperature and species concentration, microsegregation will affect the macrosegregation patterns through liquid convection and solid movement for the entire solidification system [11]. Also, if the liquid viscosity is large, viscous effects may dominate, rendering solid and liquid velocities virtually identical. If d_s is small, the difference between the solid and liquid velocities is small.

The above equation is only valid before the solid reaches the packing state, at which the pressure equilibrium assumption is no longer valid. When $g_s \geqslant g_{sp}$, the equiaxed crystals are stationary and the solid velocity is zero.

2.1.2. *Solid transport in horizontal direction.* In the absence of buoyancy forces (or other externally imposed forces), the liquid and solid momentum equations, equations (6) and (21) of ref. [1], for the horizontal direction can be expressed as

$$\frac{\partial}{\partial t}(g_l\rho_l u_l)+\nabla\cdot(g_l\rho_l \mathbf{V}_l u_l)$$
$$=-g_l\frac{\partial p_l}{\partial x}+\frac{3}{4d_s^2}(24)g_s\mu_m(u_s-u_l)$$
$$-\left(u_s-\frac{(\rho_l-\rho_s)\Gamma_s}{\rho_s\rho_l S_v^2}\frac{\partial g_s}{\partial x}\right)\Gamma_s+\nabla$$
$$\cdot\{\mu_l^*[\nabla(g_l u_l)+u_{li}\nabla g_s]\} \quad (15)$$

and

$$\frac{\partial}{\partial t}(g_s\rho_s u_s)+\nabla\cdot(g_s\rho_s \mathbf{V}_s u_s)$$
$$=-g_s\frac{\partial p_s}{\partial x}-\frac{3}{4d_s^2}(24)g_s\mu_m(u_s-u_l)$$
$$+\left(u_s-\frac{(\rho_l-\rho_s)\Gamma_s}{\rho_s\rho_l S_v^2}\frac{\partial g_s}{\partial x}\right)\Gamma_s+\nabla$$
$$\cdot\{\mu_s^*[\nabla(g_s u_s)-u_{si}\nabla g_s]\}. \quad (16)$$

If the pressure gradient in the x-direction is small relative to interfacial momentum transfer between the liquid and solid phases and inertia effects and viscous stresses are neglected, equation (16) yields the following linear relation between the solid and liquid velocities:

$$u_s=\frac{\left(\dfrac{18}{d_s^2}g_s\mu_m\right)u_l-\dfrac{(\rho_l-\rho_s)\Gamma_s}{\rho_s\rho_l S_v^2}\dfrac{\partial g_s}{\partial x}\Gamma_s}{\dfrac{18}{d_s^2}g_s\mu_m-\Gamma_s} \quad (17)$$

where the second term in the numerator is very small relative to the first term. This equation shows the effect of phase change on solid movement in the horizontal direction. If solidification is occurring ($\Gamma_s>0$), the average solid velocity exceeds the average liquid velocity. During remelting, $\Gamma_s<0$ and $u_s<u_l$. In practice, however, except for rapid solidification or remelt-

ing, the interfacial momentum transfer due to phase change is much smaller than the interfacial momentum transfer due to drag forces at the solid–liquid interface. Hence, the horizontal solid and liquid velocity components are virtually identical.

If the inertia terms are very large relative to terms associated with the viscous stress and interfacial momentum transfer due to phase change, the third and fourth terms on the right-hand side of equations (15) and (16) may be neglected. Substituting from equations (1) and (2), respectively, of ref. [1], and neglecting interfacial mass exchange due to phase change, equations (15) and (16) reduce to

$$\rho_l \frac{du_l}{dt} = -\frac{\partial p_l}{\partial x} + \frac{18}{d_s^2}\frac{g_s}{g_l}\mu_m(u_s - u_l)$$

and

$$\rho_s \frac{du_s}{dt} = -\frac{\partial p_s}{\partial x} - \frac{18}{d_s^2}\mu_m(u_s - u_l). \quad (18)$$

Eliminating the pressure gradient terms by assuming pressure equilibrium, it follows that

$$\rho_s \frac{du_s}{dt} - \rho_l \frac{du_l}{dt} = -\frac{18}{d_s^2 g_l}\mu_m(u_s - u_l)$$

$$= -\frac{18}{d_s^2 g_l}\mu_l\left(1 - \frac{g_s}{g_{sp}}\right)^{-2.5 g_{sp}}(u_s - u_l). \quad (19)$$

For constant but different phase densities, integration of equation (19) yields

$$\rho_s u_s - \rho_l u_l = (\rho_s u_s - \rho_l u_l)^0 \exp\left\{-\int_{\Delta t}\frac{18}{d_s^2 g_l}\mu_l \left(1 - \frac{g_s}{g_{sp}}\right)^{-2.5 g_{sp}} dt\right\} \quad (20)$$

where the superscript 0 stands for the previous time step. For small crystals, a large liquid viscosity, or packed solid crystals, this expression reduces to $u_s = (\rho_l/\rho_s)u_l$. Hence, for equivalent phase densities, $u_s = u_l$. If $\rho_l \neq \rho_s$, but inertia effects are also large relative to interfacial momentum transfer, the right-hand side of equation (19) is negligible and the difference between the solid and liquid velocities is equivalent to conditions at the previous time step. That is, $\rho_s u_s - \rho_l u_l = (\rho_s u_s - \rho_l u_l)^0$.

The foregoing results suggest that it is often reasonable to assume equivalent solid and liquid velocity components in the horizontal direction. The same may be said for any direction which is without buoyancy or externally applied forces.

For a general linear relation of the form,

$$\mathbf{V}_s = a\mathbf{V}_l + b \quad (21)$$

and the definition of the mixture velocity, $\mathbf{V}_m = f_l\mathbf{V}_l + f_s\mathbf{V}_s$, the following expressions may be used to relate the solid and liquid velocities to the mixture velocity

$$\mathbf{V}_s = \frac{a\mathbf{V}_m + bf_l}{f_l + af_s} \quad \text{and} \quad \mathbf{V}_l = \frac{\mathbf{V}_m - bf_s}{f_l + af_s}. \quad (22)$$

2.2. *Solutal undercooling*

Substituting equation (6) into equation (5), with the macroscopic solutal Peclet number, $Pe = \Gamma_s l_l^j/\rho_s D_l S_v$, *equated to* $\dot{R}\,\delta/D_l$, it follows that

$$\Delta f_l^\alpha = f_{si}^\alpha\left(\frac{1}{\kappa_p} - 1\right)[1 - \exp(-\Gamma_s l_l^j/\rho_s D_l S_v)]. \quad (23)$$

For large values of D_l and S_v and/or small values of l_l^j and Γ_s, $\Gamma_s l_l^j/\rho_s D_l S_v \ll 1$ and the difference between the volume-averaged liquid concentration and the interfacial liquid concentration is small ($\Delta f_l^\alpha \approx 0$). Hence, the effect of solutal undercooling is small, and the effective partition coefficient is close to the equilibrium partition coefficient ($\kappa_p^* = \kappa_p$). Such conditions exist in the interdendritic region, where the interfacial area concentration is large and the species diffusion length (which must be less than the characteristic length in that region) is small. Hence, liquid in this region can be assumed to be solutally well mixed. In the other extreme ($\Gamma_s l_l^j/\rho_s D_l S_v \gg 1$), phase change occurs rapidly, the solutal boundary layer is thick, and/or liquid species diffusion is slow. Solutal undercooling then depends on the value of the equilibrium partition coefficient, $\Delta f_l^\alpha = f_{si}^\alpha(1/\kappa_p - 1)$, and the effective partition coefficient approaches unity.

In general ($\kappa_p < \kappa_p^* < 1$), the local concentration field depends on the macroscopic solutal Peclet number, $\Gamma_s l_l^j/\rho_s D_l S_v$. In the dendritic tip region, solutal undercooling at the solidification front should be considered in predicting macrosegregation and thermosolutal convection, and its effect on macrosegregation has recently been considered for directional solidification in Pb–Sn alloys [8, 9].

Alternatively, based on an interfacial species balance [5] with negligible solid diffusion, the difference between the volume average and interfacial species concentrations of the liquid phase can be expressed as

$$\Delta f_l^\alpha = \frac{\Gamma_s l_l^j}{\rho_s D_l S_v}(f_{li}^\alpha - f_{si}^\alpha) = \frac{\Gamma_s l_l^j}{\rho_s D_l S_v}\left(\frac{1}{\kappa_p} - 1\right)f_{si}^\alpha. \quad (24)$$

Taking a Taylor series expansion of the exponential function in equation (23) and comparing with equation (24), the difference between the two solutal undercooling models is

$$\Delta\left(\frac{\Gamma_s l_l^j}{\rho_s D_l S_v}\right) = -\left(\frac{\Gamma_s l_l^j}{\rho_s D_l S_v}\right)^2\frac{1}{2!} + \left(\frac{\Gamma_s l_l^j}{\rho_s D_l S_v}\right)^3\frac{1}{3!} - \left(\frac{\Gamma_s l_l^j}{\rho_s D_l S_v}\right)^4\frac{1}{4!} + \cdots \quad (25)$$

Hence, for very small values of Pe, equations (23) and (24) are virtually equivalent.

Since solidification regions may be characterized by sharply different features, solutal undercooling may vary from one region to another, requiring some form

of model differentiation. For this purpose, four different regions are identified. They include a region with suspended or impinging equiaxed crystals, a dendrite tip region (growth front), a region of stationary packed equiaxed and columnar dendritic structures (interdendritic region), and a eutectic reaction region. These regions are illustrated schematically in Fig. 2 and may be characterized by different diffusion lengths.

2.2.1. *Liquid species diffusion length.* The liquid species diffusion length and interfacial area concentration strongly influence the macroscopic solutal Peclet number, $Pe = \Gamma_s l_l^j / \rho_s D_l S_v$, with which solutal undercooling can be computed from equation (23) or (24). Models for the liquid species diffusion length for a dispersed flow and stationary dendrites are discussed in this section, and the interfacial area concentration is treated in the next section.

For a dispersed flow with equiaxed crystals suspended in the melt [Fig. 2(a)], equiaxed growth would be impossible without undercooling of the liquid, and the phenomenon of recalescence commonly observed in castings is directly related to solutal undercooling [4]. By considering species diffusion for quasi-stationary conditions ($df_l^*/dt = 0$) and an equivalent spherical crystal, the following expression has been obtained for the liquid species diffusion length [15, 16]:

$$l_l^j = \frac{D_l}{w_e}\left\{1 - \frac{3}{g_l}\exp\left[-\left(\frac{w_e R_f}{D_l}\right)g_s^{1/3}\right] \times \int_{g_s^{1/3}}^{1} x^2 \exp\left[\frac{\left(\frac{w_e R_f}{D_l}\right)g_s^{2/3}}{x}\right] dx\right\} \quad (26)$$

where R_f is the final characteristic radius of an equivalent equiaxed crystal and w_e is the growth velocity of the characteristic envelope of the crystal, which is the growth velocity of the dendrite tips. Rappaz and Thevoz [17] represented the species diffusion length as D_l/w_e, which is a limiting case of the above result. For the limiting case, the solutal Peclet number is independent of the liquid diffusivity, which is incorrect. The growth velocity w_e may be obtained by using an interface growth kinetics model, thereby allowing the kinetics of crystal growth to be incorporated into a macroscopic solidification model. Alternatively, it may be equated to the absolute value of the mean growth rate of the liquid phase, $\mathbf{W}_l$, if the growth rate of the dendrite front is assumed to equal the mean growth rate of the solid phase in the control volume. However, since equation (26) is derived for quasi-stationary conditions ($df_l^*/dt = 0$), it does not account for the effects of convective flow and solid movement on liquid species diffusion.

Alternatively, numerous theoretical and experimental investigations have been performed to determine volumetric convection heat and/or mass transfer coefficients in dispersed flows, as well as in fluidized and packed beds. The transfer coefficients can be converted to a species diffusion length [18], and, using results obtained by Rowe and Claxton [19], Ni and Beckermann [6] obtained the following expressions for the equiaxed solidification of an Al–Cu alloy:

$$l_l^j = \frac{1 - g_s^{1/3}}{1 + \frac{(1 - g_s^{1/3})}{3g_l} Sc^{1/3} Re^a} \frac{d_s}{2} \quad (27)$$

where

$$a = \frac{2Re^{0.28} + 4.65}{3\,(Re^{0.28} + 4.65)} \qquad Sc = \frac{\nu_l}{D_l}$$

and

$$Re = \frac{g_l \rho_l |\mathbf{V}_l - \mathbf{V}_s| d_s}{\mu_l}. \quad (28)$$

Without convection, the species diffusion length reduces to $(1 - g_s^{1/3})d_s/2$, where d_s is the characteristic diameter of the suspended crystals or fragments.

Although the above model covers the range of solid fractions common to equiaxed crystals ($0 \leqslant g_s \leqslant 1$) and accounts for the effect of convection, it does not account for the effects of phase change and interface growth. Until additional research is performed to determine the effects of crystal growth rate, as well as those of convective flow and solid movement during dispersed equiaxed solidification, equations (26) and (27) provide reasonable first estimates of the species diffusion length. For suspended equiaxed crystals [Fig. 2(a) and (e)] experiencing a large growth rate, equation (26) is preferred, while for small growth rates equation (27) should be utilized.

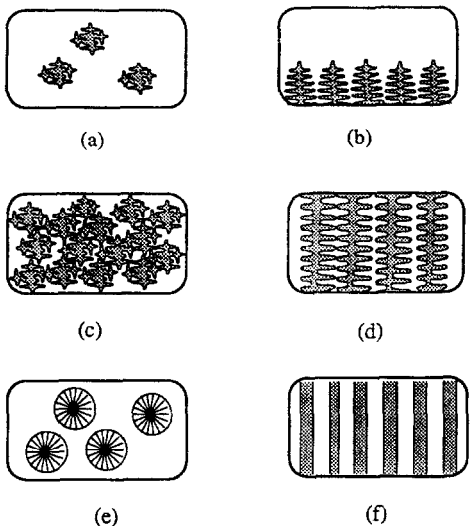

Fig. 2. Various mushy regions: (a) dispersed flow with suspended or impinging dendritic equiaxed crystals; (b) columnar dendrite tip region (growth front region); (c) and (d) interdendritic liquid region; stationary packed equiaxed crystals and columnar dendritic structures; (e) and (f) eutectic solid structure: equiaxed eutectic crystals and columnar eutectic structures.

For stationary columnar dendrites or equiaxed crystals [Fig. 2(c), (d) and (f)], the interdendritic liquid is often solutally well mixed [17, 20], and the species diffusion length is negligibly small ($l_l^i \approx 0$). In such cases it is not necessary to account for solutal undercooling. However, for a dendrite tip region [Fig. 2(b)] or a eutectic front, solutal undercooling should be considered, and for high growth rates l_l^i may be equated to D_l/w_e, with an appropriate kinetics model used to evaluate w_e. For low growth rates, equation (27) may be used by replacing d_s with the primary arm spacing λ_l.

During eutectic solidification [Fig. 2(e) and (f)], phase change takes place isothermally at the eutectic temperature and interfacial species concentrations are known. Although there is a difference between the interfacial and volume-averaged species concentrations of the liquid phase, phase change does not obey equilibrium phase relations, but is controlled by energy conservation. Therefore, in the continuum model, the value of the difference only influences the distribution of the volume averaged species concentrations of the liquid and solid phases (see equation (45) of ref. [1]).

2.3. *Topological considerations*

2.3.1. *Characteristic length of solid structures.* For equiaxed crystals, the diameter of an equivalent sphere d_s^e [Fig. 3(a)] can be introduced to represent the characteristic length d_s, where

$$d_s^e = \left(\frac{6g_s}{\pi n^V}\right)^{1/3}. \tag{29}$$

The number of crystals per unit volume n^V is the grain density, which depends on heterogeneous nucleation and fragment generation. Due to the transport of solid crystals, n^V varies across the casting domain, contributing to non-homogeneities in the final casting. Details concerning nucleation and the effects of solid movement on the distribution of n^V are presented in Section 2.4.

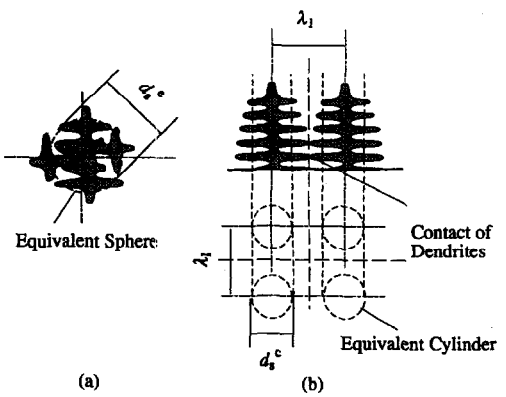

Fig. 3. Schematic illustration of equivalent spherical diameter d_s^e for equiaxed crystals and cylindrical diameter d_s^c for a square arrangement of columnar dendrites.

Similarly, columnar dendrites may be treated as equivalent cylinders [Fig. 3(b)], and the equivalent dendrite diameter (or primary dendritic arm) d_s^c can be expressed as

$$d_s^c = \left(\frac{4g_s}{\pi n^A}\right)^{1/2} \tag{30}$$

where n^A is the number of cylinder-like crystals per unit area. Since the columnar dendritic crystals are stationary, n^A is determined by heterogeneous nucleation during the early stages of solidification and remains constant. An instantaneous nucleation model developed by Stefanescu *et al.* [21] used the expression $n^A = (n^V/0.87)^{2/3}$ to relate the two grain densities. Through its influence on the initial heterogeneous nucleation, the cooling rate of a casting system determines the final size of the columnar structures. By assuming that the primary dendrite arm spacing is equal to the equivalent dendrite diameter ($\lambda_l = d_s^c$) after primary dendrites contact ($g_s = g_{scon}$), the primary arm spacing λ_l can be related to n^A and g_{scon} by the following expression:

$$\lambda_l = \left(\frac{4g_{scon}}{\pi n^A}\right)^{1/2} = 1.128\,(g_{scon})^{1/2}\left(\frac{0.87}{n^V}\right)^{1/3}. \tag{31}$$

The solid contact fraction g_{scon} is defined as the solid volume fraction at which the primary or secondary dendrite arms interact. However, if a square arrangement of columnar dendrites (Fig. 3(b)) is assumed, $\lambda_l^2 = \pi(d_s^c)^2/4 = 0.7854(d_s^c)^2$ at $g_s = g_{scon}$ and

$$\lambda_l = \left(\frac{g_{scon}}{n^A}\right)^{1/2} = (g_{scon})^{1/2}\left(\frac{0.87}{n^V}\right)^{1/3}. \tag{32}$$

Alternatively, if the dendrite trunk arrangement is assumed to be close-packed hexagonal [22], $\lambda_l^2 = 0.74316\,(d_s^c)^2$ at $g_s = g_{scon}$ and

$$\lambda_l = \left(0.7432\frac{4}{\pi}\right)^{1/2}\left(\frac{g_{scon}}{n^A}\right)^{1/2} = 0.973\,(g_{scon})^{1/2}\left(\frac{0.87}{n^V}\right)^{1/3}. \tag{33}$$

Equations (31)–(33) differ in their numerical coefficients (1.128, 1.0, and 0.973 for the foregoing dendrite arrangements, respectively), but clearly indicate that λ_l is proportional to $(1/n^V)^{1/3}$, which has been recognized in metallurgical studies of columnar solidification. Equations (31)–(33) show that the primary dendrite arm spacing is determined mainly by the system cooling rate through n^A and the interface morphology through g_{scon}. Once the solid contact fraction is obtained, the primary dendrite arm spacing λ_l can be estimated by using equation (31), (32) or (33). Conversely, since the primary dendrite arm spacing λ_l can be calculated from knowledge of the growth rate of the columnar dendrites and the temperature and concentration gradients at the columnar front [22],

the contact fraction g_{scon} could be computed from one of the foregoing λ_1–g_{scon} relations.

2.3.2. *Interfacial area concentration.* The interfacial area concentration S_v is used in a macroscopic solidification model to account for the effects of interface geometry and to provide a microstructural basis for recrystallization. It may be expressed as a function of g_s

$$S_v = a g_s^b \left(\frac{1 - \max(g_s, g_{scon})}{1 - g_{scon}} \right)^c \quad (34)$$

where the constant a depends on the number of crystals within a control volume and the exponents b and c depend on the shape of the crystals. When $g_s = 0$ or 1, $S_v = 0$. With $b = c = 1$ and $g_{scon} = 0$, equation (34) reduces to the relation proposed by Speich and Fisher [23]. However, based on the restriction that dS_v/dg_s must be infinite at $g_s = 0$ and 1, the exponents in equation (34) should be greater than zero but less than one. According to Vandermeer *et al.* [24], the exponent c is equal to $1 - b/2$, and when this relation is used with $g_{scon} = 0$, equation (34) is equivalent to the expression developed by Vandermeer *et al.* [24].

The solid contact fraction g_{scon} is introduced to account for the effects of crystal interaction. For equiaxed crystals, it is equal to the solid packing fraction g_{sp}, which is in the range from 0.6 to 0.75 [25]. For columnar crystals, the solid contact fraction is the solid fraction at which the secondary dendrite arms of adjacent crystals contact one another, and its value depends on the shape of the columnar crystals. If columnar dendrites are treated as random-packed rods, values are in the range from 0.065 to 0.907 [25]. However, additional research is needed to investigate the solid packing fraction for equiaxed crystals and the solid contact fraction for columnar dendrites. If impingement (or contact) effects are not considered, g_{scon} can be taken as zero. At the other extreme, for 'perfect' impingement of equiaxed crystals or contact of columnar dendrites occurring at the end of solidification, $g_{scon} = 1$. Such conditions never occur in practice.

The interfacial area concentration can also be expressed in terms of a characteristic length of the solid structures. Without considering impingement (or contact) effects, for equivalent spherical crystals, S_v can be expressed as [26, 27]

$$S_v = \frac{6 g_s}{d_s^e} \quad (35)$$

while for the columnar dendrites, it can be expressed as

$$S_v = \frac{4 g_s}{d_s^c}. \quad (36)$$

Substitution of equation (29) into equation (35) for equiaxed crystals gives

$$S_v = (36\pi n^v)^{1/3} g_s^{2/3}. \quad (37)$$

Although this equation does not account for impingement, it provides a limiting case of equation (34) and may therefore be used to determine the coefficient a and exponent b. It follows that $a = (36\pi n^V)^{1/3}$ and $b = 2/3$. Hence, with $c = 1 - b/2 = 2/3$, the interfacial area concentration may be expressed as

$$S_v = (36\pi n^v)^{1/3} g_s^{2/3} \left(\frac{1 - \max(g_s, g_{scon})}{1 - g_{scon}} \right)^{2/3}. \quad (38)$$

With $g_{scon} = 0$ this expression is equivalent to that proposed by Cahn [28]. A similar model with $c = (1 - g_{sp})/g_{sp}$ instead of $c = 2/3$ was also developed by Ni *et al.* [12]. This model is an extension of that originally developed by Speich and Fisher [23], and the advantages of such extensions have recently been reviewed by Bradley [29].

A similar approach can be used for columnar dendrites. By substituting equation (30) into equation (36) and comparing with equation (34), the interfacial area concentration for columnar dendrites may be expressed as

$$S_v = (4\pi n^A)^{1/2} g_s^{1/2} \left(\frac{1 - \max(g_s, g_{scon})}{1 - g_{scon}} \right)^{3/4} \quad (39)$$

where the exponent c has been taken as $1 - b/2 = 3/4$. Alternatively, the interfacial area concentration can be expressed in terms of the primary dendrite arm spacing λ_1. For example, by using equation (31), equation (39) reduces to

$$S_v = \frac{4}{\lambda_1} g_{scon}^{1/2} g_s^{1/2} \left(\frac{1 - \max(g_s, g_{scon})}{1 - g_{scon}} \right)^{3/4}. \quad (40)$$

By using equation (32), equation (39) reduces to a similar expression, except that the numerical factor 4 is replaced by $2\sqrt{\pi} \approx 3.545$, which is identical to that developed by Wang and Beckermann [15]. If equation (33) is used, the numerical factor is 3.449, rather than 4.

The foregoing topological models of dendritic characteristic lengths and interfacial area concentrations for equiaxed and columnar structures are illustrated in Fig. 4. Figure 4(a) shows results for the characteristic diameters of equivalent spherical equiaxed crystals and cylindrical columnar dendrites, normalized by final grain size and primary dendrite arm spacing, respectively. Figure 4(b) compares predictions of S_v based on equation (38), with different values of g_{scon}, and other models developed by Speich and Fisher [23] and Cahn [28]. Similar plots for the normalized effective solid–liquid interface of eutectic grains are provided by Gandin *et al.* [30] for different impingement models. Although equations (38) and (39) provide topological formulations that enable the incorporation of microstructural features in a macroscopic model of transport phenomena during solidification, areas in need of additional research relate to dendrite contact and coarsening phenomena.

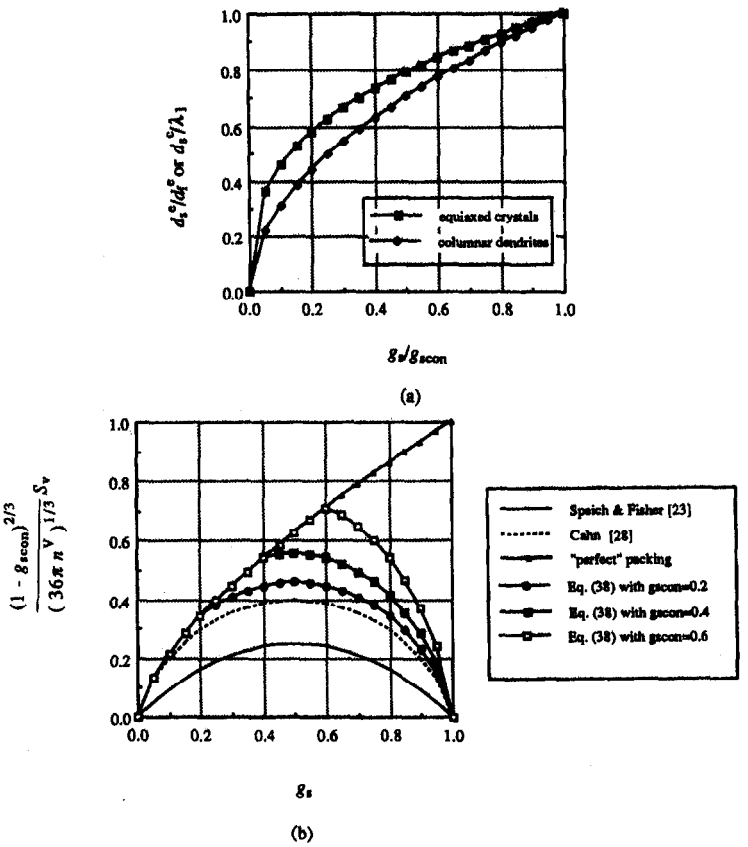

Fig. 4. Topological relations: (a) dimensionless equivalent spherical (for equiaxed crystals) and cylindrical (for columnar dendrites) diameters; (b) dimensionless area concentrations for equiaxed crystals.

2.4. *Nucleation model and prediction of final solid structure*

For stationary columnar dendrites, n^{A} is constant after heterogeneous nucleation is complete, while for moving equiaxed crystals, n^{v} varies until solidification is complete. Therefore, the grain density n^{v} depends not only on the nucleation rate during the initial stages of solidification and the fragment generation rate, but also on the advection of crystals. This feature can be characterized by a transport equation of the form [12]

$$\frac{\partial n}{\partial t}+\nabla\cdot(\mathbf{V}_s n)=\dot{n} \tag{41}$$

where n refers to n^{v} or n^{A}, for which $\mathbf{V}_s=0$. To calculate characteristic diameters and interfacial area concentrations and to predict the final sizes of equiaxed grains and/or columnar dendrites, an appropriate heterogeneous nucleation law and a model of fragment generation are needed. At this time, it is not clear how to model fragment generation and related research is clearly needed. Moreover, although detailed discussions of heterogeneous nucleation are provided by Rappaz [4] and Stefanescu *et al.* [21], at this time it is also not clear how to obtain a heterogeneous nucleation model which accounts for convection. Nevertheless, existing nucleation models provide a stepping stone for future investigations.

Because of its dependence on factors such as mold surface impurities and inclusions in the melt, as well as on melt thermophysical properties and undercooling, heterogeneous nucleation is a stochastic phenomenon. Recently, a nucleation model was developed to estimate the number of nuclei formed continuously and stochastically during the initial stages of solidification [4]. In this model, it is assumed that nucleation begins when the nucleation temperature, T_{nu}, is reached and occurs continuously until the onset of recalescence, at which point nucleation terminates. By introducing a probability function, which depends on nucleation undercooling, the number of nuclei formed per unit volume is expressed as

$$\Delta n^{\mathrm{v}}=n_{\max}\int_{\Delta T_1}^{\Delta T_2} f(\Delta T)\,\mathrm{d}(\Delta T) \tag{42}$$

where $\Delta T=T_{\mathrm{ld}}-T$ is the undercooling of the liquid melt, ΔT_1 is the undercooling of the previous time step, and ΔT_2 is the maximum undercooling associated with the end of nucleation. The probability density function is given by

$$f(\Delta T)=\frac{1}{\sqrt{(2\pi\Delta T)}}\exp\left\{-\frac{(\Delta T-\Delta T_{\mathrm{nu}})^2}{2(\Delta T_\sigma)^2}\right\} \tag{43}$$

where ΔT_σ is the standard deviation of the under-

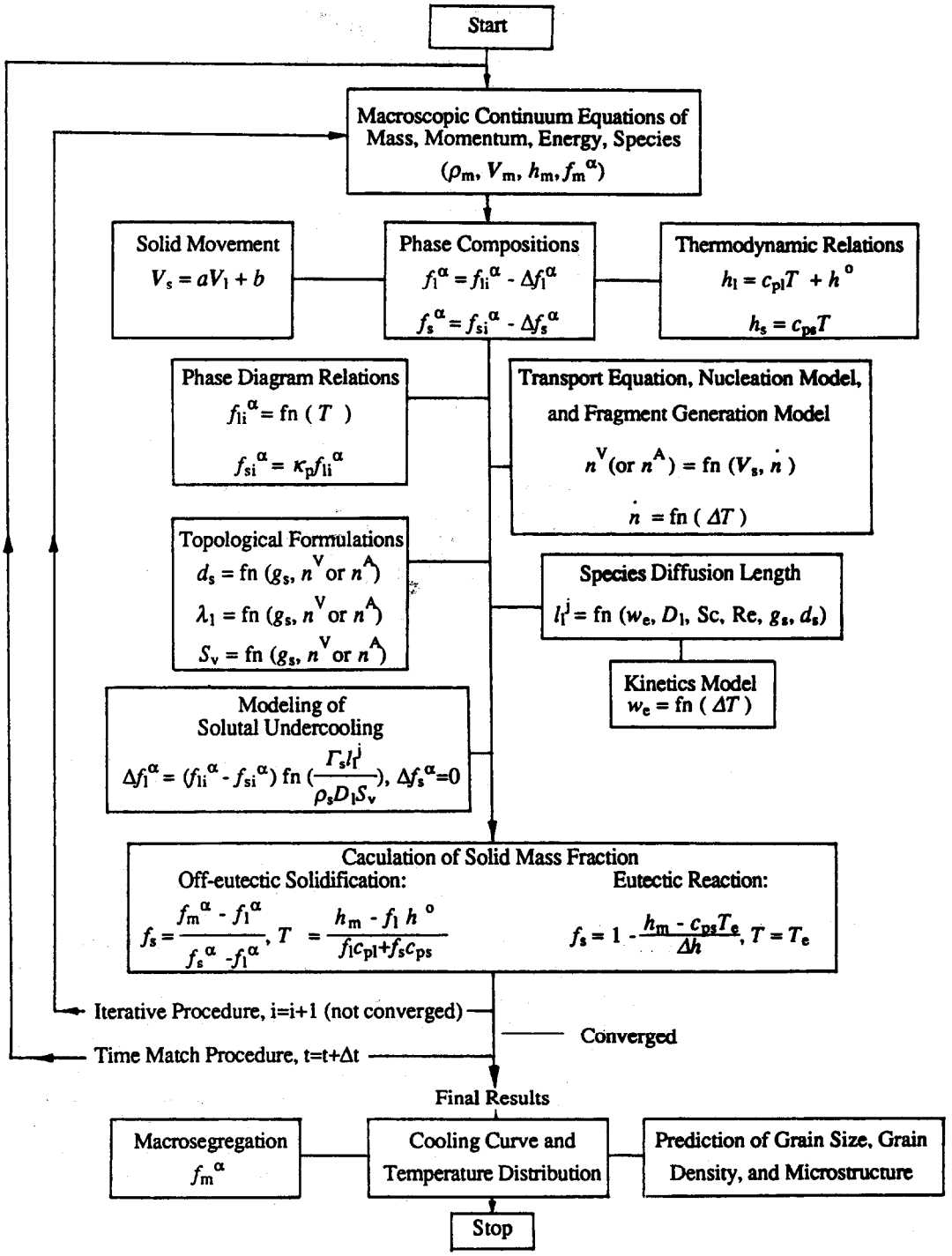

Fig. 5. Flow chart of the proposed model.

cooling and $\Delta T_{nu} = T_{ld} - T_{nu}$ is the mean nucleation undercooling. Both ΔT_σ and ΔT_{nu} may be obtained from experimental data.

Once the final number of crystals is obtained, the final grain size for equiaxed crystals and the final size of columnar dendrites can be predicted. For equiaxed crystals, from equation (29) with $g_s = g_{sp}$, the final grain size can be estimated in terms of a final grain density n_f^v. That is,

$$d_f^e = \left(\frac{6g_{sp}}{\pi n_f^v}\right)^{1/3}. \tag{44}$$

For columnar dendrites, from equation (30) with

$g_s = g_{scon}$, the final size of the solid structures can be estimated as

$$d_f^c = \left(\frac{4g_{scon}}{\pi n_f^A}\right)^{1/2} \quad (45)$$

or the primary arm spacing λ_1 can be calculated from equation (31), (32) or (33).

3. CONCLUSIONS

When used with conservation equations provided in the companion paper [1], the models of this study permit the inclusion of effects such as solid particle motion and solutal undercooling in predicting the solidification of binary mixtures. Solid motion can be determined from equation (21), with specific relations between solid and liquid velocities in the vertical and horizontal directions provided by equations (14) and (20), respectively. Solutal undercooling may be determined from equation (23) or (24), which, in turn, depend on knowledge of the phase change rate, liquid species diffusion length, liquid diffusivity, solid density, and interfacial area concentration. Two expressions, equations (26) and (27), are provided for determining the liquid species diffusion length, the first for rapid interface growth and weak convection and the second for slow interface growth and strong convection. In an interdendritic region, the liquid can be assumed to be solutally well mixed and the liquid species diffusion length is equated to zero.

Equivalent spherical and cylindrical diameters for equiaxed crystals and dendrites are introduced through equations (29) and (30), respectively, in terms of the solid volume fraction and grain density. By assuming certain dendritic trunk arrangements, the primary arm spacing can be estimated by equation (31), (32) or (33). Topological formulations for interfacial area concentrations are given by equations (38) and (39) for equiaxed solidification and columnar dendritic solidification, respectively. The topological formulations are needed to determine solutal undercooling and to predict the final size of the casting.

The foregoing characteristic lengths of the solid structures and the interfacial area concentration strongly depend on the number of crystals or dendrites, which are determined by the initial rate of nucleation and fragment generation, as well as by solid transport. A stochastic nucleation model [4] can be used to evaluate the initial nucleation rate which appears as a source term in a transport equation, equation (41), which accounts for the effects of solid movement on distribution of grain density.

A flow chart of the proposed model is provided in Fig. 5 to show the coupling between the macroscopic calculation of mass, momentum, heat and species concentration [1] and the inclusion of microscopic features such as characteristic lengths of the solid structures, interfacial geometry, interface growth, and nucleation and/or fragment generation. To successfully implement the model, criteria for delineating submodel domains, as well as characterization of numerous micro- and macro-properties, are needed. Development of such a knowledge base will require extensive experimental and numerical work.

Acknowledgements—Support of this work has been provided by the U.S. Department of Energy under Award Number DE-FG02-87ER13759. We wish to thank Dr P. J. Prescott and Mr M. J. M. Krane for reviewing the manuscript and for their many helpful comments and criticisms.

REFERENCES

1. J. Ni and F. P. Incropera, Extension of the continuum model for transport phenomena occurring during metal alloy solidification—I. The conservation equations, *Int. J. Heat Mass Transfer* **38**, 1271–1284 (1995).
2. S. C. Flood, K. Kasai and L. Katgerman, The calculation of heat, fluid flow and stress distribution during the D.C. casting of aluminum alloys. In *Numerical Methods in Thermal Problems* VI (Edited by R. W. Lewis and K. Morgan), pp. 1591–1599. Pineridge Press, Swansea (1989).
3. S. C. Flood, L. Katgerman and V. R. Voller, The calculation of macrosegregation and heat and fluid flows in the D.C. casting of aluminium alloys. In *Modeling of Casting, Welding and Advanced Solidification Processes* V (Edited by M. Rappaz, M. R. Ozgu and K. W. Mahin), pp. 683–690. TSM, Warrendale, PA (1991).
4. M. Rappaz, Modelling of microstructure formation in solidification processes, *Int. Mater. Rev.* **34**(3), 93–123 (1989).
5. J. Ni and C. Beckermann, A volume-averaged two-phase model for transport phenomena during solidification, *Metall. Trans. B* **22B**, 349–361 (1991).
6. J. Ni and C. Beckermann, Modeling of globulitic alloy solidification with convection, *J. Mater. Process. Mater. Sci.* **2**(2), 217–231 (1993).
7. M. C. Flemings, Solidification processing. In *Materials Science and Technology* (Edited by R. W. Cahn, P. Hassen and E. J. Kramer), Vol. 15, pp. 1–56. VCH, New York (1991).
8. S. N. Tewari and R. Shah, Macrosegregation during steady-state arrayed growth of dendrites in directionally solidified Pb–Sn alloys, *Metall. Trans. A* **23A**, 3383–3392 (1992).
9. S. N. Tewari, R. Shah and M. A. Chopra, Thermosolutal convection and macrosegregation caused by solute rejection at cell/dendrite tips, *Metall. Trans. A* **24A**, 1661–1669 (1993).
10. J. A. Burton, R. Prim and W. Slichter, The distribution of solute in crystal growth from the melt. Part I. Theoretical, *J. Chem. Phys.* **21**(11), 1987–1991 (1953).
11. M. C. Flemings, *Solidification Processing*. McGraw-Hill, New York (1974).
12. J. Ni, R. J. Feller and C. Beckermann, A two-phase model of transport phenomena during solidification. In *Modeling of Casting, Welding and Advanced Solidification Processes* V (Edited by M. Rappaz, M. R. Ozgu and K. W. Mahin), pp. 675–682. TSM, Warrendale, PA (1991).
13. D. B. Spalding, Computer simulation of two-phase flows, with special reference to nuclear-reactor systems. In *Computational Techniques in Heat Transfer* (Edited by R. W. Lewis, K. Morgan, J. A. Johnson and R. Smith). Pineridge Press, Swansea (1985).
14. F. Weinberg, The movement of particles in liquid metals due to gravity, *Metall. Trans. B* **15B**, 479–485 (1984).
15. C. Y. Wang and C. Beckermann, A multiphase micro-macroscopic model for solute diffusion in dendritic alloy solidification. In *Micro–macro Scale Phenomena in Sol-*

idification (Edited by C. Beckermann, L. A. Bertram, S. J. Pien and R. E. Smelser), HTD-Vol. 218/AMD-Vol. 139, pp. 43–57. ASME, New York (1992).
16. R. J. Feller and C. Beckermann, Modeling of the globulitic solidification of a binary metal alloy, *Int. Commun. Heat Mass Transfer* **20,** 311–322 (1993).
17. M. Rappaz and Ph. Thevoz, Solute diffusion model for equiaxed dendritic growth, *Acta Metall.* **35,** 1487–1497 (1987).
18. J. Ni, Development of a two-phase model of transport phenomena during equiaxed solidification, Ph.D. Thesis, The University of Iowa (1991).
19. P. N. Rowe and K. T. Claxton, Heat and mass transfer from a single sphere to fluid flowing through an array, *Trans. Inst. Chem. Engrs* **43,** T321–T333 (1965).
20. S. C. Flood and J. D. Hunt, Columnar and equiaxed growth, *J. Crystal Growth* **82,** 543–551 (1987).
21. D. M. Stefanescu, G. Upadhya and D. Bandyopadhyay, Heat transfer solidification kinetics modeling of solidification castings, *Metall. Trans A* **21A,** 997–1005 (1990).
22. W. Kurz and D. J. Fisher, *Fundamentals of Solidification.* Trans. Tech. Publications, Adermannsdorf (1989).
23. G. R. Speich and R. M. Fisher, Recrystallization of a rapidly heated 3.25% silicon steel. In *Recrystallization, Grain Growth and Textures*, pp. 563–598. ASM, Metal Park, OH (1966).
24. R. A. Vandermeer, R. A. Masumura and B. B. Rath, Microstructural paths of shaped-preserved nucleation and growth transformations, *Acta Metall.* **39**(3), 383–389 (1991).
25. L. E. Nielson, *Polymer Rheology*. Marcel Dekker, New York (1979).
26. R. B. Bird, W. E. Stewart and E. N. Lightfoot, *Transport Phenomena*. Wiley, New York (1960).
27. R. T. DeHoff and F. N. Rhines, *Quantitative Microscopy*. McGraw-Hill, New York (1968).
28. J. W. Cahn, The significance of average mean curvature and its determination by quantitative metallography, *TMS-AIME* **239,** 610 (1967).
29. F. J. Bradley, A stereological formulation for the source term in micromodels of equiaxed eutectic solidification, *Metall. Trans. B* **24B,** 539–544 (1993).
30. Ch. A. Gandin, Ch. Charbon and M. Rappaz, Probabilistic modeling of grain formation in solidification processes. In *Modeling of Casting, Welding and Advanced Solidification Processes*—VI (Edited by T. S. Piwonka, V. Voller and K. Katgerman), pp. 21–28. TSM, Warrendale, PA (1993).